CHALMERS
UNIVERSITY OF TECHNOLOGY

Comparative analysis of cathode morphologies in structural batteries using X-ray absorption near edge spectroscopy (XANES) and electrochemical

Downloaded from: https://research.chalmers.se, 2025-01-15 15:56 UTC

Citation for the original published paper (version of record):
Barthelay, T., Gray, R., Richards, H. et al (2025). Comparative analysis of cathode morphologies in structural batteries using X-ray absorption
near edge spectroscopy (XANES) and electrochemical methods. Journal of Power Sources, 630.
http://dx.doi.org/10.1016/j.jpowsour.2024.236050

N.B. When citing this work, cite the original published paper.

research.chalmers.se offers the possibility of retrieving research publications produced at Chalmers University of Technology. It covers all kind of research output: articles, dissertations, conference papers, reports etc. since 2004. research.chalmers.se is administrated and maintained by Chalmers Library

(article starts on next page)

Journal of Power Sources 630 (2025) 236050

Contents lists available at ScienceDirect

Journal of Power Sources

journal homepage: www.elsevier.com/locate/jpowsour

Comparative analysis of cathode morphologies in structural batteries using X-ray absorption near edge spectroscopy (XANES) and electrochemical methods

Thomas Barthelay [a,b,*], Robert Gray [a], Howard Richards [a], Paloma Rodriguez Santana [a], Sylvia Britto [c], Kalotina Geraki [d], Zhenyuan Xia [e], Johanna Xu [e], Leif E. Asp [e], Chris Bowen [a], Frank Marken [f], Alexander Lunt [a], Andrew Rhead [a,**]

[a] Department of Mechanical Engineering, The University of Bath, Claverton Down, Bath, UK
[b] Department of Materials, University of Oxford, Oxford, OX1 3PH, UK
[c] STFC, Rutherford Appleton Laboratory, ISIS Facility, Chilton, UK
[d] Diamond Light Source, Harwell Science and Innovation Campus, Didcot, Oxfordshire, UK
[e] Department of Industrial and Materials Science, Chalmers University of Technology, Gothenburg, Sweden
[f] Department of Chemistry, University of Bath, Claverton Down, Bath, UK

HIGHLIGHTS

- Morphology of cathode on surface of carbon fibres affect battery performance.
- Thick, uneven slurry coating improves lithium access in the cathode.
- Homogenous coating provides more stable half-cell cycling.
- Inhomogeneous coating leads to higher resistances for each cell component

GRAPHICAL ABSTRACT

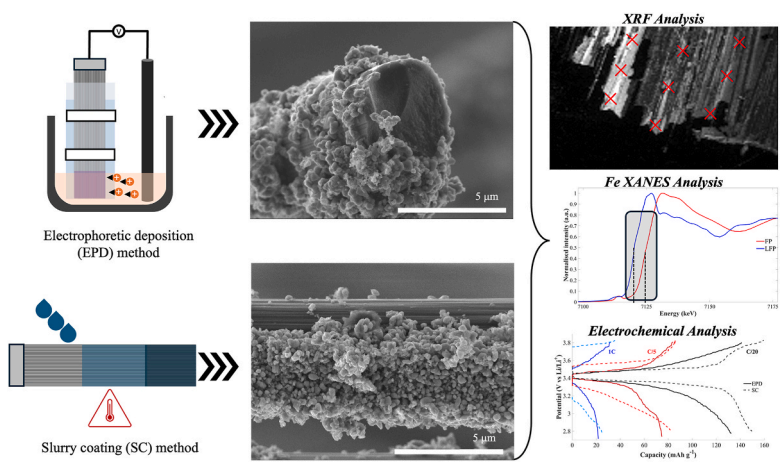

ABSTRACT

Structural batteries utilise the bifunctionality of carbon fibres to act as a load-bearing structure, but also as a conductive current collector for a battery electrode. Lithium-ion transport during the cycling of structural battery cathodes coated with different morphologies is investigated using Iron X-Ray Absorption Near Edge Spectroscopy (Fe XANES) and correlated to electrochemical performance. Two contrasting morphologies were produced using slurry coating and electrophoretic deposition (EPD) of lithium-iron phosphate (LFP) onto continuous carbon fibres. The ability to study the different structural battery cathode morphologies *operando*

* Corresponding author. Department of Materials, University of Oxford, Oxford, OX1 3PH, UK.
** Corresponding author. Department of Mechanical Engineering, The University of Bath, Claverton Down, Bath, UK.
E-mail addresses: thomas.barthelay@materials.ox.ac.uk (T. Barthelay), A.T.Rhead@bath.ac.uk (A. Rhead).

https://doi.org/10.1016/j.jpowsour.2024.236050
Received 25 October 2024; Received in revised form 6 December 2024; Accepted 9 December 2024
Available online 3 January 2025
0378-7753/© 2024 The Authors. Published by Elsevier B.V. This is an open access article under the CC BY license (http://creativecommons.org/licenses/by/4.0/).

allows for a comparative analysis of their impact on cycling performance. The EPD-coated fibres exhibited a more homogeneous, thinner coating around the fibre compared to the thick, one-sided coating produced using slurry coating. Despite a lower initial capacity and 30 % lithium re-intercalation loss in the first cycle, EPD-coated fibres exhibited more stable capacity retention over time compared to slurry-coated counterparts. Electrochemical Impedance Spectroscopy (EIS) revealed initially high ionic resistance for the EPD-coated fibres, but a larger increase in resistance in the slurry coated electrodes over multiple cycles. This study demonstrated an innovative and novel method of analysing in greater detail, the cycling ability of the coated cathode material on carbon fibres using synchrotron radiation.

1. Introduction

Lightweight energy storage has been a focal point for researchers who aim to realise electrified air travel and more efficient electric vehicles [1]. Current methods utilise external components to strengthen the battery pack, such as polyurethane (PU) honeycomb designs, which are encapsulated within aluminium/steel sheets or thin-films lithium batteries between carbon fibre structures [2]. While these advanced structures offer improved mass savings of up to 10 %, further improvements are required to achieve the higher energy density demands for aerospace [3]. One particularly promising route involves combining the monofunctional mechanical structure and electrochemical material into a single multifunctional system, which has the potential to increase efficiency by up to 26 % [4].

Multifunctional structural batteries therefore aim to combine the mechanical properties of a load-bearing structure with the electrochemical capabilities of a conventional lithium-ion battery cell. There have been a number of iterations of the multifunctional batteries that utilise carbon fibre materials [5–11] with a laminated architecture being one of the first examples of its kind [12]. This battery architecture utilises a carbon fibre anode, biphasic polymer electrolyte [13,14], glass fibre separator and lithium-iron-phosphate (LFP)/aluminium substrate cathode material. The resulting devices possess an energy density of 24 Wh kg^{-1} and elastic modulus of 25 GPa, from which the mechanical properties arise primarily from the thin and high stiffness separators and the relatively thick negative carbon fibre anode [15,16], and not from the positive LFP/aluminium cathode. An alternative approach to achieving a positive electrode is to use coated carbon fibres that also offer mechanical support along with the carbon fibre-based anode, as opposed to using a conventional aluminium coated electrode [17,18].

Efficiently coating the electrodes is of vital importance to the performance. Electrophoretic deposition (EPD) provides an efficient, scalable and flexible route for coating the complex shapes of carbon fibres, compared to other electrode coating methods [11,19]. Successful attempts at coating carbon fibres using this method have previously demonstrated its effectiveness, such as work conducted by Hagberg et al. [20] whose use of EPD with LFP particles, PVDF binder, and carbon black additives, achieved good adhesion of particle to the fibre surface and electrical connectivity. Sanchez et al. [21] enhanced the process by using exfoliated graphene oxide, changing solvents, and eliminating the need for PVDF, resulting in reduced deposition time, higher capacities, and better cycle retention. Despite its advantages of thickness tunability, EPD is time-intensive and not yet adopted for mass manufacturing, warranting exploration of alternative scalable methods.

Slurry coating is an alternative approach to produce coated carbon fibre and is a common commercial process for coating lithium-ion battery electrodes [22,23]. It entails applying a solution with the active material, binder, and conductive additives onto a 2D current collector, followed by solvent evaporation to leave a solid cathode material. Recent research has developed slurry coating methods for coating individual carbon fibres and has resulted in the first structural battery that utilises both a structural anode and cathode [24,25]. The 3-dimensional shape and irregular spacing of individual fibres led to inadequate coverage and adhesion of the active material, resulting in lower capacity compared to conventional aluminium/copper sheet electrodes. To improve this method of coating a carbon fibre, there is a need to understand how these inherent properties of the fibres influence the electrochemical capabilities of the active materials.

X-ray absorption near-edge spectroscopy (XANES) is used to analyse the lithium distribution within a cathode material during a charge cycle [26,27]. By studying the absorption edge of transition metals within the electrode, which reflects the element's oxidation state, it is possible to determine how much lithium can be found within the electrode. Cathode coated carbon fibres have not been studied to this level of detail previously and by using this technique, it will be possible to determine how cathode morphology affects lithiation.

This paper explores the two most prevalent manufacturing methods of coating lithium-iron phosphate active material onto the surface of individual carbon fibres, slurry coating and electrophoretic deposition. Electrochemical characterisation was performed in a pouch cell with a lithium-metal counter electrode and liquid electrolyte. Electrochemical characterisation was performed via X-ray absorption near-edge spectroscopy (XANES), which was complemented by an electron microscopy study of the two coated electrodes in order to understand the influence of the coating morphology on electrochemical performance. By tracking the phase change of the coated LFP during de/lithiation, and its influence on cathode performance, this work elucidates the importance of cathode morphology to the electrical connectivity between the active material and the carbon fibre current collector. Results in this paper will support future specific tailoring of not only structural battery cathodes, but all cathodes that use a 3-dimensional current collector support.

2. Materials and methods

2.1. Materials

Unsized polyacrylonitrile(PAN)-based carbon fibres (T800SC-24K separated by weight to a 3K tow, Toray) were used for slurry coated fibres whilst T800SC-12k-50C fibres that were desized were used for EPD, following the procedure in Sanchez et al. [21]. The two different coating methods, slurry coating and electrophoretic deposition, were performed using the same materials where possible. Two different types of $LiFePO_4$ (LFP) were used, a smaller 80–100 nm particle size was used for electrochemical testing (>99 %, Nanoshel) to improve lifetime performance, while a larger particle size of <5 mm (>97 %, Sigma) was used for the synchrotron experiment for enhanced X-ray interaction. The exfoliated graphene oxide (EGO) was prepared using a method based on direct exfoliation of graphite flakes, as reported by Xia et al. [28]. Carbon black, Super P Conductive (>99 %, Alfa Aesar) was used for both samples. Each carbon fibre sample was weighed before coating and held between two glass slides, leaving a single side exposed for coating and another for electrical connection, as shown in Fig. 1(a).

2.2. Preparation of electrode slurry coating

For the slurry coating procedure, a slurry solution was made using 100 mL 1-methyl-2-pyrrolidone, (NMP) (>99.5 %, Sigma-Aldrich) containing LFP (500 mg), 25 mg EGO, 25 mg CB and 50 mg of PVDF (Sigma-Aldrich). The slurry was stirred for 1 h and subsequently ultrasonicated for 20 min before 2.5 mL of the solution was pipetted onto the exposed section of the carbon fibre. The coated fibres were then immediately placed in a 200 °C oven for 1 h and heated under vacuum at 110 °C overnight.

2.3. Preparation of electrophoretic deposition

An electrophoretic deposition (EPD) suspension was made by slowly adding 500 μl PDDA (20%wt in water) (Sigma) to 100 ml of absolute ethanol, which was chosen as an alternative to previously used DMF or acetone as a more sustainable choice of solvent [29,30]. LFP (500 mg), EGO (25 mg) and CB (25 mg) were then added to the ethanol solution and stirred for 1 h to create the suspension, as depicted in Fig. 1(b). No binder was required for this procedure.

For the electrodeposition process, a 3k carbon fibre tow was inserted between two vertically offset glass slides, after ensuring the fibres were flat and had 1 cm of fibre exposed, as shown in Fig. 1 (a). The carbon fibre tow was then connected to an aluminium strip using silver paint which was dried for 1 h at 50 °C to ensure all solvent had evaporated. Before the electrodes were submerged in the EPD suspension, it was ultrasonicated for 20 min. The carbon fibre working electrode was then placed in the EPD suspension 2.5 cm from the graphite counter electrode. The working electrode was connected to the negative terminal of a bench-top power supply, with the counter electrode connected to the positive terminal. A potential difference of 70 V applied between the electrodes, as shown in Fig. 1 (b). Deposition time was 300 s. Following deposition, the sample was placed in an oven at 110 °C for 15 h under vacuum.

2.4. Pouch cell assembly

To create the pouch cell, the dried electrodes, formed by slurry coating or electrophoretic deposition were introduced into a glovebox (Vigor) with argon atmosphere (<1 ppm H_2O and O_2). A half-cell set up was made using a 1 cm wide lithium-metal strip (Sigma, 99.9 %) used a counter electrode, which covered the exposed area of carbon fibre coated in lithium-iron phosphate (LFP). A 250 μm thick glass microfibre filter (Whatman) separator was employed between the LFP working electrode and Li-metal counter electrode. The electrolyte used for all samples consisted of equal parts ethylene carbonate (EC) (Sigma-Aldrich, 99 %) and propylene carbonate (PC) (Sigma- Aldrich, >99 %) and 0.4M:0.6M bis(oxalato)borate (LiBoB) (Sigma-Aldrich):Lithium trifluoromethanesulfonate (LiTFS) (Sigma-Alrichm, >99 %). The cell was filled with 0.5 mL of electrolyte before being heat sealed, with the final half-cell layout shown in Fig. 1 (c).

2.5. Electrochemical characterisation

The cells were galvanostatically cycled using a potentiostat (Metrohm Micro-Autolab III, Nova Software) between 2.8 V and 3.8 V vs Li/Li^+ for a range of C-rates, from C/20, C/10, C/5, C/2 to 1C before being cycled back at C/20 for 5 cycles at each C-rate. The cell was then cycled for a further 20 cycles at C/2 to measure the stability at a relatively high charge rate. The cycling current was calculated by using the initial mass of the uncoated carbon fibres which was subtracted from the final mass of the coated electrode to find the mass of the coating.

To analyse the different coatings on each electrode, a two-electrode half-cell setup was employed to exclusively focus on the active material. Lithium metal was used to serve as both the reference and counter electrode in this configuration. Given the surplus of lithium in the counter electrode compared to the working electrode, the lithium metal remains constant throughout the cycling process. EIS testing was conducted using a potentiostat (Solatron Analytical ModuLab XM MTS system) connected to the current collectors of the working and counter electrodes. Each cell was cycled galvanostatically at a charge rate of C/10 for 5 cycles and then a further cycle at C/2, with an EIS frequency sweep conducted at every 25 % state of charge (SOC) increment. Galvanostatic measurements maintain a constant current throughout the experiment, while variables such as voltage were adjusted. The sweep amplitude was set to 10 mV relative to the open-circuit potential, with start and end frequencies at 100 kHz and 1 Hz, respectively. The frequency sweep followed a logarithmic scale with 10 points per decade. The LFP cells underwent six galvanostatic charges, reaching 100 % SOC when the cell voltage hits 4 V vs Li/Li^+ and discharged to 0 % SOC when the cell voltage reaches 2.8 V vs Li/Li^+. The resulting Nyquist plots were then fitted using an equivalent circuit model (ZView, Scribner Associates, Inc.).

2.6. Synchrotron cell setup and characterisation

X-Ray Fluorescence (XRF) and XANES were performed on the I18 microfocus spectroscopy beamline at Diamond Light Source, Oxford, UK to map the LFP particles and to understand the extent of lithiation of the coated LFP particles, respectively. Half-cell samples were mounted into a motorised co-axially fixed tower that held the samples in place during analysis and could be moved and rotated to ensure good coverage of the working electrodes. A Si(111) monochromator was used to select an incident beam energy for analysis and Kirkpatrick–Baez Si mirrors were used to focus the beam to a 10 × 10 μm^2 spot size for the XRF and 2 × 2 μm^2 spot for the XANES. The smaller spot size used for XANES was used to obtain a higher signal-to-noise ratio and increase the accuracy of the measurements. An 8 keV energy was used for the XRF measurements with two Vortex Silicon detectors. A small, motorised stage was able to raster the sample to perform mapping of each of the samples, as shown schematically in Fig. 2 (a). XANES was performed at selected locations within each 2D map obtained by XRF to evaluate the electron charge state of the elements as shown in Fig. 2 (c) and the subsequent XANES profiles with corresponding rising edge shown in Fig. 2 (d).

To carry out a combination of XANES and X-Ray Fluorescence (XRF)

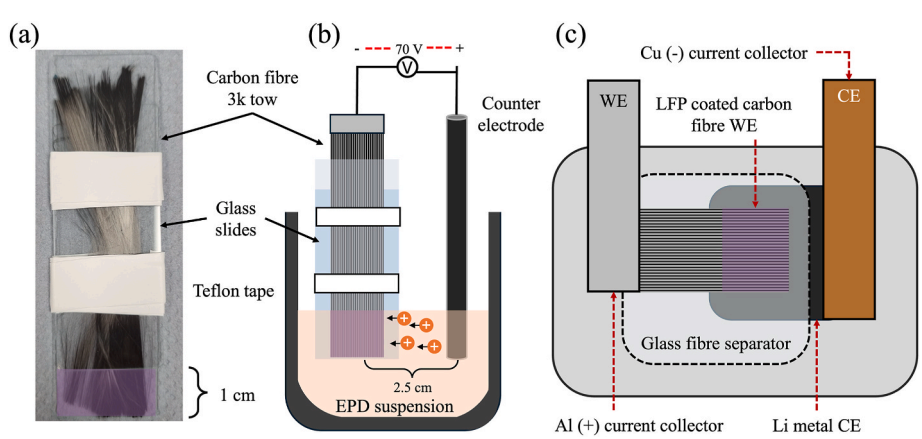

Fig. 1. (a) Example of prepared working carbon fibre electrode before coating. (b) Graphical depiction of electrophoretic deposition (EPD) experimental setup. (c) Graphical depiction of half-cell layout.

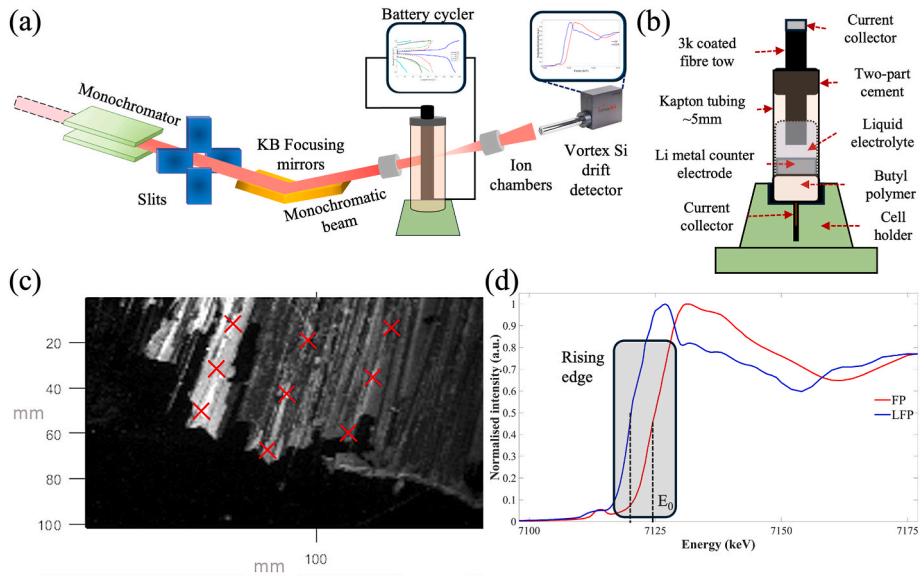

Fig. 2. (a) Schematic of XANES and Fe-XRF beamline setup at I18, Diamond Light Source, UK. (b) Novel cylindrical cell design for operando testing of LFP coated carbon fibre half-cells in Kapton tubing. (c) Example of Fe-XRF image of immersed LFP coated carbon fibre. d) Examples of XANES spectra of lithiated (blue) and delithatied (red) lithium iron phosphate with example of rising edge profile and calculated edge value (E_0).

on the active material, whilst protecting the components in the cell from air and moisture, a novel cylindrical shaped battery cell was constructed; see Fig. 2 (b) The cell was sealed in a 5 mm thick walled Kapton tube, in an argon atmosphere, using two-part epoxy putty (Sylmasta AB). A lithium metal counter electrode was sealed on one side using a commercial butyl polymer (Tacky Tape) that was resistant to dissolution, as shown in Fig. 2 (b). Three cells were made using the electrophoretically deposited fibres (denoted by EPD_x, where x is the charge rate) and one cell was made using the slurry coated fibres (denoted by SC_x). The coated fibres were then placed in the cylindrical cell design and filled with the bespoke LiTFS/LiBoB electrolyte so that the 1 cm of coated fibre was submerged. Prior to XANES analysis, each cell was cycled through 5 charge/discharge cycles (except EPD_P due to it being a pristine cell) at their respective charge rates, C/10 for $EPD_{C/10}$ and $SC_{C/10}$, and C/5 for $EPD_{C/5}$ as describe in Table 1.

Each sample was placed onto a co-axially fixed tower to allow for full rotation of the specimen during analysis; this allowed for optimal orientation of fibre for detailed XANES analysis. An initial Fe X-ray fluorescence (Fe-XRF) image was taken of the sample to locate spots of high Fe concentration as shown in Fig. 2 (c), where brightness indicates the concentration of Fe. For each sample, nine points were chosen from three vertical lines along single fibres that showed a high and consistent iron concentration, determined using the Fe-XRF maps where brighter pixels indicated higher Fe concentration, indicated by red crosses in Fig. 2 (c). Following this, XANES characterisation was performed over a full charge and subsequent discharge cycle in increments of 20 % capacity, with the charge held constant during data collection. The starting energy of the sweep was at 7000 eV and increased in increments of 5 eV, until the pre-edge energy of 7090 eV where the increments decreased to 1 eV and finally 0.5 eV at 7110 eV. The size of the increments then increased after the K-edge peak at 7170 eV–1 eV, with intensity of a specific energy being measured by signal emitted from the sample.

Table 1
Pre-cycling information for carbon fibre coated LFP samples (EPD - Electrophoretic Deposition, SC - Slurry coated).

Sample	No. of pre-cycles	Charge rate	Capacity retention (%)	Coating method
EPD_p	0	–	–	EPD
$EPD_{C/10}$	5	0.1	78.3	EPD
$EPD_{C/5}$	5	0.2	74.5	EPD
$SC_{C/10}$	5	0.1	82.7	SC

3. Results and discussion

3.1. Electrode morphology

Following the electrochemical deposition using electrophoretic deposition (EPD), the morphology of the fibre coating was examined using a Scanning Electron Microscopy (SEM, JEOL JSM7900F), as shown in Fig. 3. A 10 keV was used for the fibres set in epoxy (Fig. 3 (a)) and 5 keV for the raw fibres (Fig. 3(b) and (c)). This revealed a varying coating thickness across fibres, with some regions of coating exceeding 10 μm while others being less than 2 μm thick. However, for the EPD coated fibres showed a relatively consistent coating over the whole circumference was observed, as shown in Fig. 3 (a). Differences in thickness are attributed to uneven current distribution due to sub-optimal electrical connectivity between fibres and the voltage source.

Agglomerations of fibres sharing LFP were observed, resulting in enhanced electrical connections and thicker coatings on some fibres, while others lacked coating altogether. While cross-sectional analysis revealed the coating around the fibre was not consistent, this may have been dislodged during the cutting process.

The EPD coating fibres were also analysed using SEM, which showed that the agglomeration of the active material is supported around the circumference of the fibres, as shown in Fig. 3 (a). While slurry coating, commonly used for 2D materials, such as aluminium or copper sheets in commercial batteries, it is less suitable for 3D materials. Direct application of slurry coating to the front face of individual fibres resulted in uneven and one sided coating, with a maximum thickness of approximately 1 μm and the reverse face mostly uncoated, as shown in Fig. 3 (b)–and (c).

3.2. X-ray absorption near-edge spectroscopy (XANES) analysis

The shift in the XANES rising edge (E_0) was calculated for each 2 × 2 μm^2 spot at every state-of-charge for all samples using linear combination fitting in the Athena software package [31]. Two control XANES

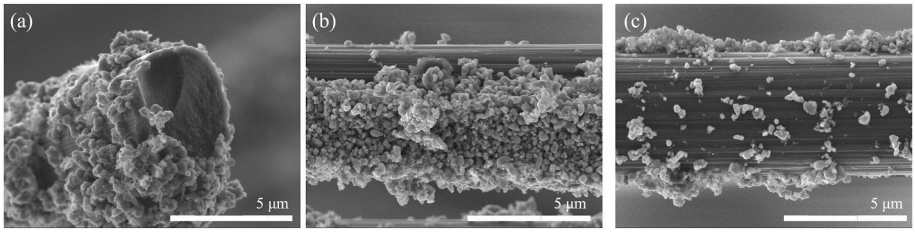

Fig. 3. (a) A cross-sectional SEM images of electrophoretically deposited carbon fibres cut using liquid nitrogen and a doctor blade. (b) Front side of the slurry coated carbon fibre showing thick coating that does not encompass the full circumference of the fibre. (c) Reverse side of the slurry coated carbon fibre showing minimal coating.

spectra were obtained to use as reference materials. For fully delithiated and lithiated control samples, $FePO_4$ powder and a LFP coated carbon fibre sample were held between two sheets of Kapton tape subjected to the same conditions as those used for collecting XANES spectra from the battery cells. For maximum lithium content (x = 1) in Li_xFePO_4, the E_0(LFP) was 7120.0 eV. For minimum lithium content (x = 0), the E_0(FP) was 7123.5 eV. These values were obtained by finding the steepest gradient in the leading edge. Both spectra showed strong agreement with previous studies [26,32]. To monitor the progression of lithiation and delithiation during cycling, lithium content was derived directly from the E_0 values of each sample. The average and standard deviation of the nine spectra were then plotted against the corresponding state-of-charge.

Fig. 4 (a) shows the change of lithium content during the first cycle at a charge rate of C/2 for a pristine EPD Li_xFePO_4 electrode, as the concentration falls from $x = 0.94$ at 0 % SOC to $x = 0.29$, revealing ~70 % lithium utilization during the initial charging; the 100 % data point appears anomalous. After delithiation, full lithiation is not regained and lithium content only reaches $x = 0.69$ during the charge. This 30 % total capacity loss is attributed to the formation of a cathode electrode interphase (CEI) on the LFP particles, loss of active LFP material, or lithium metal counter electrode dendrite formation. After being cycled five times at a lower C-rate of C/10, the initial and final lithium content after the full cycle remain similar, Fig. 4 (b) shows the cathode material recovering Li^+ to the same original level ($x = 0.60$). Enhanced capacity retention in $EPD_{C/10}$ is attributed to limited lithium loss during the 6th cycle, despite the higher C-rate cycling of C/2, demonstrating the active material's charge retention at lower rates.

When cycled at a higher C-rate of C/5, shown in Fig. 4 (c), the lithium content in fully discharged state (0 % in $EPD_{C/5}$) is higher ($x = 0.70$) than $EPD_{C/10}$ ($x = 0.60$). A similar trend is observed in fully charged state (80 %/100 %), where the lowest lithium content in the $EPD_{C/5}$ ($x = 0.39$) is larger than the lowest for $EPD_{C/10}$ ($x = 0.33$). This indicates faster cycling utilises less lithium by the active material than slower rates over multiple cycles, meaning that the $EPD_{C/5}$ cell has a lower final capacity than the $EPD_{C/10}$, as quantified in Table 1. Importantly, the lithium content recovered to its original level even after this cycle, demonstrating that the faster charge rate does not affect the ability of the active material to recover lithium.

On comparing electrophoretically deposited ($EPD_{C/10}$) and slurry-coated ($SC_{C/10}$) samples under the same cycling conditions, the slurry-coated cathode demonstrated an improved ability to access more lithium during this cycle. Large discrepancies in the margin of error from arise from the uneven lithiating/delithiating of the individual fibres and

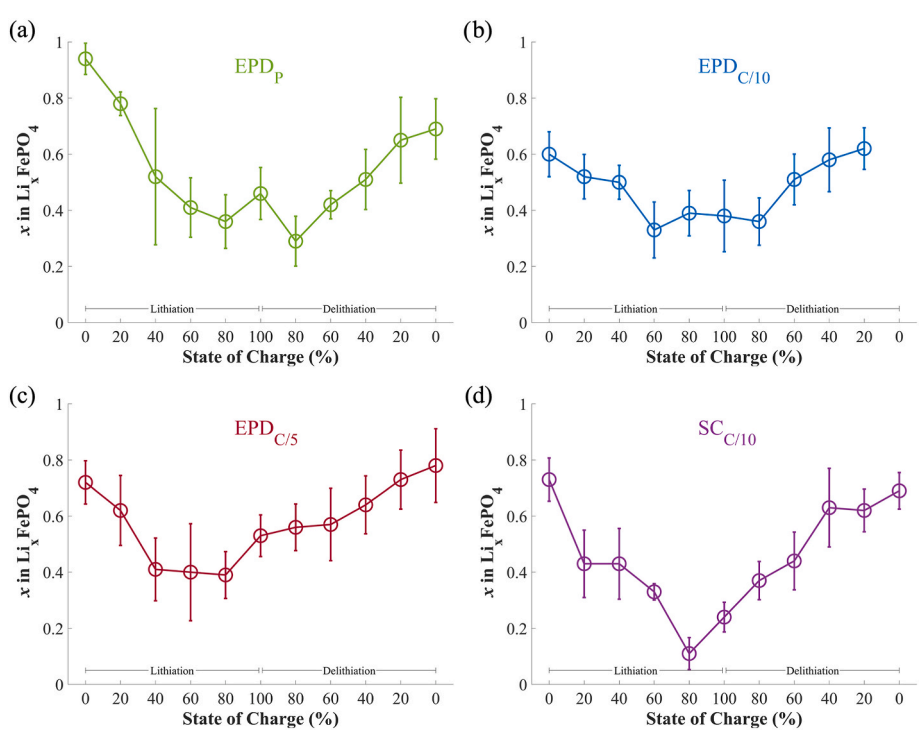

Fig. 4. Lithium-ion content in the LFP electrode at different states of charge for samples analysed by XANES, with the range of lithium content for each sample. E – EPD made cells, S - slurry coated cells. (a) Pristine EPD coated cell with no previous cycling, (b) EPD cell previously cycled at C/10, (c) EPD cell previously cycled at C/5 and (d) slurry coated cell previously cycled at C/10, all for 5 cycles.

is attributed to why the lowest lithium content is not always at 100 % state of charge in Fig. 4. The initial discharged state of the $SC_{C/10}$ has a higher lithium content of $x = 0.73$ compared to $x = 0.6$ of the $EPD_{C/10}$ sample, see Fig. 4 (d). In addition, Fig. 4 (d) shows that more lithium is removed from the cathode material for the slurry-coated sample than the electrophoretic deposited. This indicates that the "charged" state of the slurry-coated fibre has significantly lower lithium content ($x = 0.11$ at 80 %) than the lowest lithium content "charged" state of the EPD sample ($x = 0.33$ at 60 %). In additional, the slurry coated sample has a better electrically connected network between the active LFP particles and the carbon fibre current collector. This is thought to be due to better mixing of the solvent in the slurry coating method, thereby resulting in the exfoliated graphene oxide being more distributed within the active material.

In the slurry coated sample, the lithium content between the initial zero state of charge ($x = 0.73$) and the final zero state of charge ($x = 0.69$) is a greater fall loss than for the EPD sample. This indicates some capacity loss, which can arrive from a stable passivation layer that is not fully formed, resulting in the decrease in charge capacity after the first five cycles. This is thought to be due to the high density of the slurry coating sample, which results in greater particle fracturing and loss of active material. This can cause the increase in overpotential, the difference in measured potential and open-circuit potential during cycling, and therefore lower the capacity. Another cause of lithium loss is the formation of CEI, and this may be exacerbated in the slurry coated sample by the fracturing of particles leading to newly exposed LFP surface, resulting in higher CEI growth, compared to that of the more evenly and thinner coated EPD samples [33].

$$Error(\varepsilon) = \sigma/\sqrt{N} \qquad \text{Equation 1}$$

Whilst charging and discharging of all the cathodes, the lithium content is unevenly distributed through-out the coated cathode which results in a range of lithiation state, as shown in Fig. 4. This can be quantified by averaging the errors for each sample, calculated using Equation (1):

where σ is the standard deviation for each point in the sample, and N is the number of data points taken from the sample. For each sample, the error values across all SOC were averaged to determine the unitless variance of lithiation ($\bar{\varepsilon}$), which is shown in Table 2. The first cycle of the pristine sample, EPD_P, has one of the largest range of values of 0.103, which indicates that during the first cycle, the distribution of oxidised active particles is uneven. This is thought to be caused by structural changes that occur during the first cycle of delithiation and then lithiation, leading to less lithium being able to return to the cathode material, as well as the formation of the electrode/electrolyte interphase [34]. These structural changes occur over several cycles until there is little change in the difference in the composition and a more consistent coulombic efficiency is observed. For example, the LFP particles in sample $EPD_{C/10}$ appear to have a more consistent LFP/FP conversion during cycling compared to the pristine sample, as seen in Fig. 4(a) and (b). The effects of structural changes are less pronounced in the slurry-coated sample $SC_{C/10}$, with the lowest variance of all the samples at 0.083. This means that the change in LFP/FP particles is more homogenous across the electrode during cycling. Using the higher charge rate of C/5 compared to C/10, shown in $EPD_{C/5}$ sample, leads to more localised changes in lithium-ion concentration and results in a high LFP/FP disparity across the electrode. This can be attributed to the uneven distribution of particles across the electrode, where the difficulty to oxidise/reduce particles that are less accessible for the lithium-ion is exacerbated when cycling the LFP at a higher C-rate [26]. This results in the higher degree of fluctuation of Li + distribution at higher C-rates due to an inconsistent coating, where regions with poor connectivity will not be lithiated/delithiated as easily.

Improving the resolution of this technique would lead to improved results and an ability to better analyse the surface. Due to the thin electrode coatings and shape of the carbon fibres, only few sections were able to be studied for each sample. Potentially thicker coatings would aide in the ability to study the lithiation of the electrodes, however this may worsen the performance of the electrode itself [21] and not be a realistic comparison to a real electrode.

Table 2
Lithium content distribution for each sample analysed using XANES.

Sample	EPD_P	$EPD_{C/10}$	$EPD_{C/5}$	$SC_{C/10}$
Li + distribution - $\bar{\varepsilon}$ a.u.	0.103	0.093	0.109	0.083

3.3. Pouch cell performance

Both the slurry cast, and EPD coated carbon fibre electrodes were used in a half-cell pouch cell, which is shown schematically in Fig. 1 (c). The electrodes were galvanostatically rate-tested against a lithium-metal counter electrode for 30 cycles at different C-rates of C/20, C/10, C/5, C/2, 1C and then C/20 for a second time in 5 cycle segments. The cells were then cycled for an extended 20 cycles at C/2.

For the EPD sample, cycling at different C-rates (as shown in Fig. 5 (a) reveals a 9 % capacity decrease from 132.4 mAh g^{-1} to 120.6 mAh g^{-1} (decrease of 11.8 mAh g^{-1}) during the initial C/20 cycles, indicating the formation of a CEI. Subsequent C/10 cycling results in a 20 mAh g^{-1} capacity drop from C/20 with similar trends occur at C/5, although with an initially high first charge due to less efficient discharges compared to C/10. Higher C-rates (C/2 and 1C) exhibit lower coulombic efficiency, showing a reduced LFP utilization compared to slower rates. However, returning to C/20 cycling after high C-rate tests results in nearly complete capacity retention (0.25 % reduction).

The EPD cell was then cycled at C/2 for an additional 20 cycles to assess extended-term stability, with capacity results shown in Fig. 5 (a). The first discharge capacity of long-term cycling was 37.5 mAh g^{-1}, declining by 9.6 mAh g^{-1}, 25.6 %, to 27.9 mAh g^{-1} after 20 cycles. The

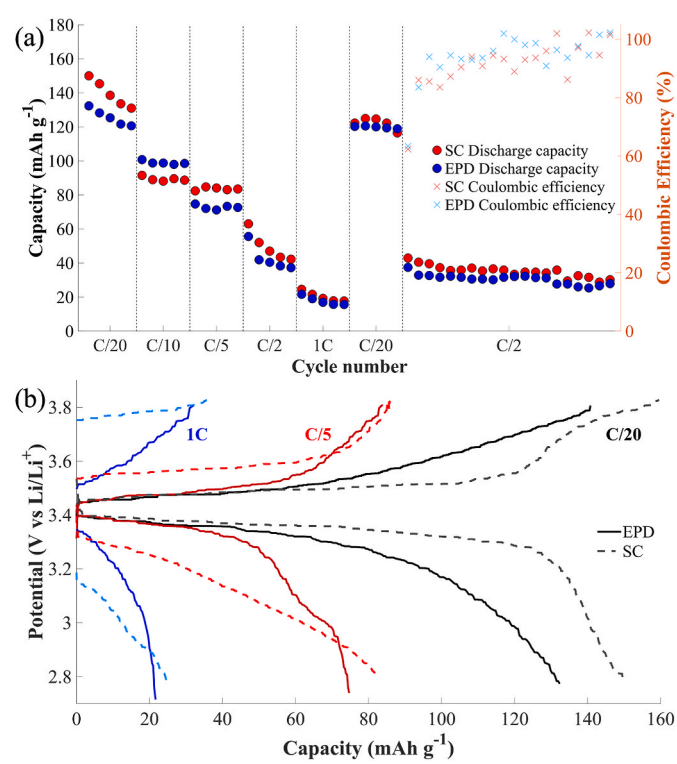

Fig. 5. (a) Combined discharge capacities of a sequential cycling cascade of LFP half-cells, deposited using EPD and SC. (b) Voltage charge and discharge profile for different charging rates for EPD and SC coated carbon fibres.

stability of these cycles is not constant but has coulombic efficiency that is greater than 90 % for almost all the cycles.

The cycling behaviour of the slurry coated fibres are also shown in Fig. 5 (a). The comparisons between this cell and EPD coated fibres revealed similar trends due to the use of the same cathode material. However, slurry-coated fibres consistently exhibited higher initial discharge capacities across most charge rates, apart from at C/10. For example, at C/20, the initial discharge capacity was 150.0 mAh g^{-1}, surpassing the discharge capacity of 132.4 mAh g^{-1} of the EPD electrode. Despite the higher capacities, the slurry-coated electrode experienced a greater capacity drop of 33.5 mAh g^{-1}, with a final discharge capacity of 116.5 mAh g^{-1} at C/20 compared to 117.9 mAh g^{-1} for the EPD-coated electrode.

The slurry-coated electrode underwent the same 20 cycles as the EPD-coated sample at a C-rate of C/2 resulting in a final discharge capacity of 30.2 mAh g^{-1}, representing a 29.8 % reduction from the initial discharge capacity of 43.0 mAh g^{-1} for the 20-cycle run. The coulombic efficiency fluctuates for both samples but is more pronounced in the slurry-coated electrode, with a standard deviation of the coulombic efficiencies for the extended cycles of 5.63 %, compared to that of 4.55 % for the EPD sample. The coulombic efficiency for the first cycle is low due to previous cycle having a lower C-rate and was there excluded. This adds to the evidence of the higher instability in the slurry-coated cell compared to the EPD cell. This higher instability of discharge capacity in the slurry-coated cell causes a steeper fall in discharge capacity during these 20 cycles compared to that in the more stable EPD cell. Having a more homogenous cathode coating and, therefore, stable electrode is vital for future development of structural batteries to ensure improved longevity of the cell.

The first charge and discharge curves for each C-rate are shown in Fig. 5 (b), providing insight into electrochemical behaviour. Rate-limiting processes induce overpotential, reducing specific capacity and widening the voltage gap between charge and discharge profiles. Initial overpotential for C/20 is attributed to first cycle CEI formation on LFP surface. The curves for each C-rate show the same shape, albeit with higher overpotentials and more extreme cut-offs for the faster charge rates.

Voltage profiles of slurry-coated fibres Fig. 5 (b) show overpotentials increasing with higher charge rates, leading to an elevation in cell potential and obscuring characteristic curves; this is particularly evident at higher currents. Overpotentials for slurry-coated cathodes demonstrate a notable increase with rising C-rate, with an approximate tenfold rise from C/20 to 1C. This change is more pronounced than the profiles in the EPD, indicating that the thick, inhomogeneous coating of the LFP on the surface of the slurry coated carbon fibre suffers from higher resistances at higher C-rates than the coating of the EPD samples.

The electrochemical performance of these electrodes is compared to literature values for electrodes prepared using similar techniques in Table 3. The results align with the findings of this study, where the slurry-coated electrode exhibits a higher initial capacity, but poorer capacity retention compared to the electrodes prepared by electrophoretic deposition.

Table 3
Comparison of electrode electrochemical performance with literature. *Measured from the first C/2 cycle.

	Initial discharge capacity (mAh g^{-1})	High C-rate discharge capacity (mAh g^{-1})	Long term retention (%)
EPD – **this work**	132 (C/20)	25 (1C)	50 (45 cycles @ C/2)*
SC – **this work**	150 (C/20)	22 (1C)	48 (45 cycles @ C/2)*
EPD – Sanchez et al. [21]	131 (C/10)	86 (1C)	91 (500 cycles @ 1C)
SC – Choi et al. [19]	144 (C/10)	~105 (1C)	81 (300 cycles @ 1C)

While the discharge capacity of the electrodes in this work is lower than reported in other studies, the focus here is to investigate the impact of morphology whilst minimizing variations in other parameters. This approach sacrifices optimization of individual electrodes but enables a more detailed analysis of the factors contributing to the observed discrepancies.

3.4. Electrochemical impedance spectroscopy (EIS) measurements

Separate EPD and slurry cast cells were manufactured to analyse their performance using electrochemical impedance spectroscopy. The cells were cycled for five cycles at C/10 and then for a cycle at C/2 to mimic the conditions of cells XANES. Nyquist plots were generated for each sample during the first two C/10 cycles and the final C/2 cycle. An example Nyquist plot for an EPD carbon fibre cathode is shown in Fig. 6 (a). Each of these Nyquist plots were processed in order to generate equivalent circuit models (ECM) and quantify the circuit component values associated with an equivalent Nyquist plot. A double RC circuit, composed of two superimposed semi-circles and a Warburg element representing the diffusion at lower frequencies, best characterized the electrochemical setup as shown in shown in Fig. 6 (b).

Table 4 provides an overview of the metrics that statistically measure the '*goodness of fit*' for each equivalent circuit model, χ^2 and the Total Sum of Squares (TSS). These results demonstrate that the quality of fit is over a magnitude better for a double RC circuit fit than the fit for a single RC circuit. Therefore, a double RC circuit ECM was used to characterise all SOCs.

The results from the Nyquist plot analysis for the EPD sample, shown Fig. 7(a–c) and the slurry cast sample, shown in Fig. 7(d–e). R_Ω, R_1 and R_2 represent the internal ohmic resistance of the cell, charge-transfer resistance and electrode diffusion resistance, respectively, and each component of the cells can be compared to assess these electrochemical phenomena that occur within the half-cells.

During the initial charge, there was a noticeable decrease in resistance across all equivalent circuit models components for the EPD coated cell, indicating CEI formation at the electrode/electrolyte interface, which facilitates easier Li^+ movement. However, if the CEI becomes too thick or traps lithium atoms, it can disrupt electrical connectivity due to changes in cathodic material morphology, which is often observed after extended cycling or in the presence of impurities.

R_1, as shown in Fig. 7 (b), initially remained stable during the first charge cycle. However, this sample demonstrated a significant increase

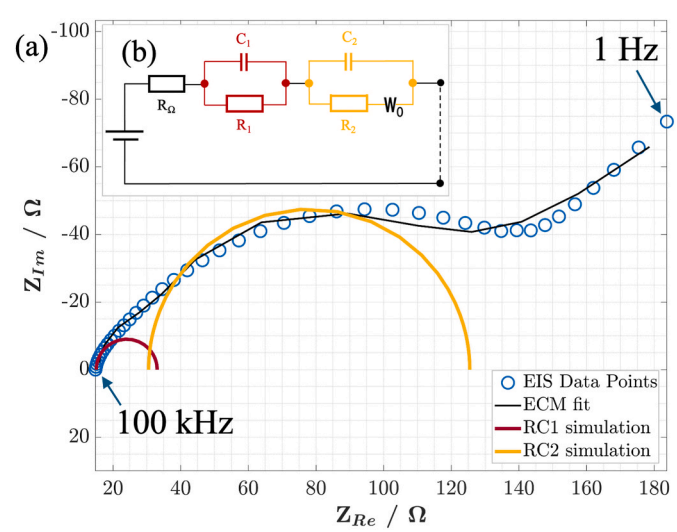

Fig. 6. The Nyquist plot (a) and the corresponding equivalent-circuit model (ECM) (b) for a pristine EPD coated fibre half-cell. Red semi-circle and yellow semi-circle is represented by the red and yellow RC circuit, respectively.

Table 4
Comparison of the statistical values to determine 'goodness of fit' for the EIS plot of the pristine EPD sample.

Type of ECM	χ^2	TSS
Single RC circuit	0.0090	0.261
Double RC circuit	0.0006	0.059

in the second discharge, indicating an increased resistance from the growth of a CEI. In the 6th cycle, both the charge and discharge showed elevated resistance due to higher current rates, with R_1 resistance decreasing slightly, suggesting minimal CEI layer thinning after cycling.

Similar patterns were observed in R_2, as shown in Fig. 7 (c), with the resistance increasing during discharge. This is likely due to difficulties in lithium ions intercalating into the cathode crystal structure at higher Li^+ concentrations. A general trend of increasing resistance was also observed, most likely due to cathode material degradation associated with fractures and delaminations, that in turn leads to a more complex pathway for lithium-ion movement within the cathode.

The Nyquist plots of slurry-coated fibres closely resembled those of EPD-coated fibres, indicating similar electrochemical behaviour. However, the resistances were notably higher for the slurry-coated fibres with similar coated weights. This is thought to be due to differences in coating thickness and concentration, affecting charge-transfer reactions, as seen in Fig. 3 (a). This corresponds with observed high overpotentials from voltage profiles in Fig. 5 (b).

In Fig. 7 (d), the R_Ω ECM element exhibited consistent resistance during low C-rate cycles 1 and 2. A higher C-rate of C/2 led to an elevated resistance, which remained constant through charge and discharge, despite a substantial 0 %–25 % resistance drop, indicating an initial higher internal resistance.

The R_1 resistance gradually increased across all cycles for the slurry coated sample, with a significant rise in the final two C/2 cycles as shown in Fig. 7 (e). This indicates a consistent CEI build-up accelerated by high C-rate. Charge cycles were generally found to be associated with a resistance decrease, while discharge cycles showed a resistance increase due to CEI formation. R_2 resistance decreased during charge cycles and increased during discharge as shown in Fig. 7 (f), mirroring the EPD trend. Faster C/2 cycles exhibited lower R_2 resistance compared to slower C/10 cycles, due to either material loss during cycling or the inaccessibility of LFP particles. Due to the thick and agglomerated slurry-coated particles, any dislocation or loss of electrical contact can increase resistance. This is because the reduced lithium-ion flux, caused by the lesser available active material for lithiation, results in lower capacity over time.

Electrophoretic deposition and slurry-coating have both clear strengths and weaknesses when being used for structural battery cathode production. Electrophoretic deposition enables a more controlled and homogeneous coating of the carbon fibres, which results in an improved life cycle of the electrode, as shown by electrochemical impedance spectroscopy and cycling testing. However, EPD offers a lower initial capacity than that of the slurry-coated electrode due to the improved distribution of particles within the uneven coating of the slurry-coated electrode. The slurry-coating method is a much faster and easier coating method that is already using in conventional electrode manufacturing. Further research into the conductive properties of various morphologies would provide valuable insights into the effects of coating method on electrode performance. Equally, computational studies employing multi-physics modelling would enhance the understanding of key features such as porosity, tortuosity, and potential electronic changes associated with each morphology. From this work, utilising 3-dimensional carbon fibres rather than the conventional 2-dimensional aluminium sheets for these electrodes alters the performance significantly. To fully optimise these structural electrodes, either a new coating procedure is required to allow for slurry-coating to allow for a homogenous coating or a combinate of electrophoretic deposition with a slurry-coating method is needed to maximise the performance of both methods. In future work, in order to confirm the stability of these materials, structural and morphological analysis of the structural changes in morphology of the electrodes from charging/discharging cycles, both with and without the SEI should be conducted.

4. Conclusions

This work successfully examined lithium-ion transport during long-term cycling of structural battery cathodes, correlating electrochemical performance to the morphology of active material deposited by two methods: electrophoretic deposition (EPD) and slurry coating. An even, homogenous coating around the circumference allows for a more stable cathode, compared to an uneven, highly dense coating promotes

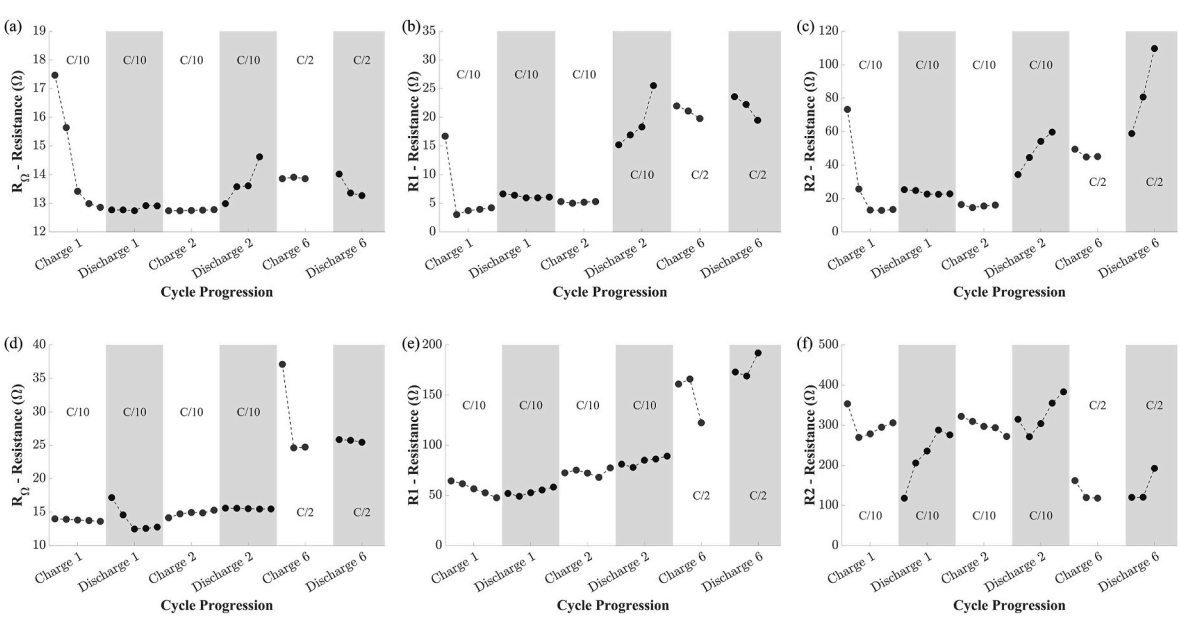

Fig. 7. Resistance changes over the equivalent circuit model components over the first, second and sixth cycles for the EPD coated cell shown in (a) R_Ω, (b) RC1 and (c) RC2 and for the slurry-coated cell shown in (d) R_Ω, (e) RC1 and (f) RC2.

high initial capacity but with higher degradation with increased cycling.

Electron microscopy of the coated carbon fibres using the slurry coating methodology results in an inhomogeneous coating around the circumference of the carbon fibre. This occurs as only part of the three-dimensional surface area is exposed to the slurry during coating. This contrasts with the electrophoretic deposition methodology, which can coat the total circumference of the fibre.

A novel *operando* technique was developed to study the extent of lithiation in the cathode coating using synchrotron radiation for XANES analysis. This approach enabled precise tracking of particle lithiation at various locations within the electrode. Coupled with electrochemical techniques, this method allowed for a comprehensive assessment of the performance differences arising from different morphologies arising from two coating techniques. Electrophoretic deposition, which applies a uniform coating around the entire circumference of the electrode, resulted in a more stable and less resistive electrode. In contrast, the slurry coating method produced a one-sided, denser layer that offered a higher initial discharge capacity but led to greater capacity loss over multiple cycles and increased overpotentials at higher C-rates, attributed to higher internal resistances. This is reflected by cycling results showing slurry cast coating having an initially higher discharge capacity (150.0 mAh g^{-1}) during cycling than the EPD coating (132.4 mAh g^{-1}). However, over extended cycling, this coating suffers from higher capacity fade of 29.8 % over extended cycling of 20 cycles at C/2 compared to 25.6 % for the EPD coating. To ensure a longer performing structural battery, it would therefore be best to use EPD coating due to having lower degradation with slurry coating being used for higher capacity requirements over a shorter lifetime.

For the first time, key electrochemical differences of two distinct cathode coating methods, onto three-dimensional current collector substrates, have been studied with distinct benefits of each. Understanding morphology of these coatings provides insight into the need for improved techniques for ensuring a uniform and consistent coating to enhance long-term performance and stability of structural battery cathodes.

CRediT authorship contribution statement

Thomas Barthelay: Writing – review & editing, Writing – original draft, Visualization, Project administration, Methodology, Investigation, Formal analysis, Data curation, Conceptualization. **Robert Gray:** Methodology, Investigation. **Howard Richards:** Investigation. **Paloma Rodriguez Santana:** Methodology. **Sylvia Britto:** Supervision, Methodology. **Kalotina Geraki:** Supervision, Methodology. **Zhenyuan Xia:** Investigation. **Johanna Xu:** Writing – review & editing, Investigation. **Leif E. Asp:** Writing – review & editing. **Chris Bowen:** Writing – review & editing. **Frank Marken:** Writing – review & editing, Supervision, Methodology, Conceptualization. **Alexander Lunt:** Writing – review & editing, Supervision, Methodology, Funding acquisition, Conceptualization. **Andrew Rhead:** Writing – review & editing, Supervision, Methodology, Funding acquisition, Conceptualization.

Declaration of competing interest

The authors declare the following financial interests/personal relationships which may be considered as potential competing interests: Thomas Barthelay reports financial support was provided by GKN Aerospace Services Limited. Rob Gray reports financial support was provided by GKN Aerospace Services Limited. Paloma Santana Rodriguez reports financial support was provided by GKN Aerospace Services Limited. If there are other authors, they declare that they have no known competing financial interests or personal relationships that could have appeared to influence the work reported in this paper.

Acknowledgements

This work was financially supported by Engineering and Physical Sciences Research Council Centre for Doctoral Training in Advanced Automotive Propulsion Systems (AAPS), under the project EP/S023364/1. Financial support was also provided by GKN Aerospace. Additional support was provided by the 2DTECH VINNOVA Competence Centre (Ref. 2019-00068), the USAF EOARD (Award No. FA8655-21-1-7038), and the ONR, USA (Award No. N62909-22-1-2037). Diamond Light Source is acknowledged for providing the beamtime on I18 beamline under the experiment number SP30127. The authors also gratefully acknowledge Matthew Frost and Teiin Carbon Europe GmbH for supplying carbon fibre material.

Data availability

Data will be made available on request.

References

[1] D. Carlstedt, L.E. Asp, Performance analysis framework for structural battery composites in electric vehicles, Compos. B Eng. 186 (2020) 107822.
[2] T. Jin, G. Singer, K. Liang, Y. Yang, Structural batteries: advances, challenges and perspectives, Mater. Today 62 (2023) 151–167.
[3] A. Bills, S. Sripad, W.L. Fredericks, M. Singh, V. Viswanathan, Performance metrics required of next- generation batteries to electrify commercial aircraft, ACS Energy Lett. 5 (2020) 663–668.
[4] W. Johannisson, et al., A residual performance methodology to evaluate multifunctional systems, Multifunctional Materials 3 (2020) 025002.
[5] H. Zhou, et al., Structural composite energy storage devices — a review, Mater. Today Energy 24 (2022) 100924.
[6] H.W. Park, M.S. Jang, J.S. Choi, J. Pyo, C.G. Kim, Characteristics of woven carbon fabric current collector electrodes for structural battery, Compos. Struct. 256 (2021) 112999.
[7] F. Danzi, et al., Structural batteries: a review, Molecules 26 (2021) 2203, 26, 2203 (2021).
[8] T. Pereira, Z. Guo, S. Nieh, J. Arias, H.T. Hahn, Embedding thin-film lithium energy cells in structural composites, Compos. Sci. Technol. 68 (2008) 1935–1941.
[9] J.P. Thomas, S.M. Qidwai, W.R. Pogue, G.T. Pham, Multifunctional structure-battery composites for marine systems, J. Compos. Mater. 47 (2013) 5–26.
[10] K. Moyer, et al., Carbon fiber reinforced structural lithium-ion battery composite: multifunctional power integration for CubeSats, Energy Storage Mater. 24 (2020) 676–681.
[11] Gray, R. et al. Carbon fibre based electrodes for structural batteries. J Mater Chem A Mater 6, 4883–5230.
[12] L.E. Asp, et al., A structural battery and its multifunctional performance, Advanced Energy and Sustainability Research 2 (2021) 2000093.
[13] N. Ihrner, W. Johannisson, F. Sieland, D. Zenkert, M. Johansson, Structural lithium ion battery electrolytes via reaction induced phase-separation, J Mater Chem A Mater 5 (2017) 25652–25659.
[14] S. Duan, et al., Three-dimensional reconstruction and computational analysis of a structural battery composite electrolyte, Communications Materials 4 (1) (2023) 1–9, 2023 4.
[15] G. Fredi, et al., Graphitic microstructure and performance of carbon fibre Li-ion structural battery electrodes, Multifunctional Materials 1 (2018) 015003.
[16] S. Duan, et al., Effect of lithiation on the elastic moduli of carbon fibres, Carbon N Y 185 (2021) 234–241.
[17] J. Chen, et al., Carbon fiber reinforced Zn–MnO2 structural composite batteries, Compos. Sci. Technol. 209 (2021) 108787.
[18] N.A.A. Sutrisnoh, G.J.H. Lim, K.K. Chan, J.J.N. Lim, M. Srinivasan, Structural cathodes: navigating the challenges in fabrication and multifunctional performance analysis, Compos. Sci. Technol. 242 (2023) 110147.
[19] J. Choi, O. Zabihi, M. Ahmadi, M. Naebe, Advancing structural batteries: cost-efficient high-performance carbon fiber-coated LiFePO 4 cathodes, RSC Adv. 13 (2023) 30633–30642.
[20] J. Hagberg, et al., Lithium iron phosphate coated carbon fiber electrodes for structural lithium ion batteries, Compos. Sci. Technol. 162 (2018) 235–243.
[21] J.S. Sanchez, et al., Electrophoretic coating of LiFePO4/Graphene oxide on carbon fibers as cathode electrodes for structural lithium ion batteries, Compos. Sci. Technol. 208 (2021) 108768.
[22] P.S. Grant, et al., Roadmap on Li-ion battery manufacturing research, J. Phys.: Energy 4 (2022) 042006.
[23] C.D. Reynolds, P.R. Slater, S.D. Hare, M.J.H. Simmons, E. Kendrick, A review of metrology in lithium-ion electrode coating processes, Mater. Des. 209 (2021) 109971.
[24] H.W. Park, M.S. Jang, J.S. Choi, J. Pyo, C.G. Kim, Characteristics of woven carbon fabric current collector electrodes for structural battery, Compos. Struct. 256 (2021) 112999.

[25] Q. Jiang, A. Beutl, H. Kühnelt, A. Bismarck, Structural composite batteries made from carbon fibre reinforced electrodes/polymer gel electrolyte prepregs, Compos. Sci. Technol. 244 (2023) 110312.
[26] J. Wang, Y.C.K. Chen-Wiegart, J. Wang, In operando tracking phase transformation evolution of lithium iron phosphate with hard X-ray microscopy, Nat. Commun. 5 (1) (2014) 1–10, 2014 5.
[27] S. Yang, et al., Soft X-ray XANES studies of various phases related to LiFePO4 based cathode materials, Energy Environ. Sci. 5 (2012) 7007–7016.
[28] Z.Y. Xia, et al., A robust, modular approach to produce graphene–MO x multilayer foams as electrodes for Li-ion batteries, Nanoscale 11 (2019) 5265–5273.
[29] C. Capello, U. Fischer, K. Hungerbühler, What is a green solvent? A comprehensive framework for the environmental assessment of solvents, Green Chem. 9 (2007) 927–934.
[30] Z. Xia, et al., Green synthesis of positive electrodes for high performance structural batteries - a study on graphene additives, Compos. Sci. Technol. 251 (2024) 110568.
[31] B. Ravel, M. Newville, ATHENA, ARTEMIS, HEPHAESTUS: data analysis for X-ray absorption spectroscopy using IFEFFIT 12 (2005) 537–541, urn:issn:0909-0495.
[32] N. Nihlatunnur, C. Latif, V.S.I. Negara, W. Wongtepa, S. Pratapa, Fe K-Edge X-ray absorption Near-Edge spectroscopy and morphology analyses of LiFePO4 powders, Mater. Today Proc. 44 (2021) 3361–3364.
[33] E.R. Logan, et al., The effect of LiFePO4 particle size and surface area on the performance of LiFePO4/graphite cells, J. Electrochem. Soc. 169 (2022) 050524.
[34] M.V. Blanco, et al., Simultaneous monitoring of structural changes and phase distribution of LiFePO4 along the cathode thickness of Li metal polymer battery, J. Electrochem. Soc. 167 (2020) 160517.